

AD-A042 162

NAVAL RESEARCH LAB WASHINGTON D C
DIFFUSION OF MAGNETIC FLUX INTO A CYLINDRICAL LINER IN THE LIM--ETC(U)
MAY 77 A L COOPER, D L BOOK

F/G 20/3

UNCLASSIFIED

NRL-MR-3507

NL

| OF |

ADA042162



END

DATE
FILMED

8-77

AD A 042162

[Handwritten signature]

[Handwritten signature]

NRL Memorandum Report 3507

Diffusion of Magnetic Flux into a Cylindrical Liner in the Limit of High Magnetic Reynolds Number

A. L. COOPER AND D. L. BOOK

Plasma Physics Division

May 1977



DDC
RECEIVED
JUL 26 1977
D

[Handwritten signature]

NAVAL RESEARCH LABORATORY
Washington, D.C.

AD No. _____
DDC FILE COPY

SECURITY CLASSIFICATION OF THIS PAGE (When Data Entered)

9 REPORT DOCUMENTATION PAGE		READ INSTRUCTIONS BEFORE COMPLETING FORM
1. REPORT NUMBER NRL Memorandum Report 3507	2. GOVT ACCESSION NO.	3. RECIPIENT'S CATALOG NUMBER
4. TITLE (and Subtitle) DIFFUSION OF MAGNETIC FLUX INTO A CYLINDRICAL LINER IN THE LIMIT OF HIGH MAGNETIC REYNOLDS NUMBER		5. TYPE OF REPORT & PERIOD COVERED Interim report on a continuing NRL problem.
7. AUTHOR(s) A.L. Cooper and D.L. Book		6. PERFORMING ORG. REPORT NUMBER
9. PERFORMING ORGANIZATION NAME AND ADDRESS Naval Research Laboratory Washington, D.C. 20375		8. CONTRACT OR GRANT NUMBER(s)
11. CONTROLLING OFFICE NAME AND ADDRESS Energy Research and Development Administration Washington, D.C. 20545		10. PROGRAM ELEMENT, PROJECT, TASK AREA & WORK UNIT NUMBERS NRL Problem H02-37 Project ERDA-E(49-20)-1009(81706)
14. MONITORING AGENCY NAME & ADDRESS (if different from Controlling Office) 12 Hq.		12. REPORT DATE May 1977
		13. NUMBER OF PAGES 49
		15. SECURITY CLASS. (of this report) UNCLASSIFIED
		15a. DECLASSIFICATION/DOWNGRADING SCHEDULE
16. DISTRIBUTION STATEMENT (of this Report) Approved for public release; distribution unlimited. 14 NRL-MR-3507		
17. DISTRIBUTION STATEMENT (of the abstract entered in Block 20, if different from Report)		
18. SUPPLEMENTARY NOTES		
19. KEY WORDS (Continue on reverse side if necessary and identify by block number)		
20. ABSTRACT (Continue on reverse side if necessary and identify by block number) 1/(square root of Rm) Calculations have been made of the rate at which confined magnetic flux compressed by an imploding cylindrical liner diffuses into the latter because of finite electrical resistivity. The diffused magnetic field profile and associated magnetic energy and Joule heating are also calculated. In the limit of high magnetic Reynolds number R_m , the skin depth, total diffused flux and associated energy scale like $R_m^{-1/2}$. It is shown that cylindrical liner motion mitigates the diffusion calculated in slab models, owing to the reduction in the surface area through which the flux must diffuse. The influence of the form of the liner trajectory on the results is displayed.		

DD FORM 1 JAN 73 1473

EDITION OF 1 NOV 65 IS OBSOLETE
S/N 0102-014-6601

SECURITY CLASSIFICATION OF THIS PAGE (When Data Entered)

251 950

LB

ACCESSION for	
NTIS	White Section <input checked="" type="checkbox"/>
DDC	Bull Section <input type="checkbox"/>
UNANNOUNCED	<input type="checkbox"/>
JUSTIFICATION.....	
BY.....	
DISTRIBUTION/AVAILABILITY CODES	
Dist.	AVAIL. and/or SPECIAL
A	

CONTENTS

I. INTRODUCTION	1
II. DERIVATION OF THE FORMALISM	5
III. LARGE MAGNETIC REYNOLDS NUMBER	11
IV. NUMERICAL RESULTS	16
V. CONCLUSION	20
ACKNOWLEDGMENT	20
APPENDIX — The Convection-Diffusion Problem in Slab Geometry	21
REFERENCES	27

DDC
 RECEIVED
 JUL 26 1977
 RECEIVED
 D

DIFFUSION OF MAGNETIC FLUX INTO A CYLINDRICAL LINER IN THE LIMIT OF HIGH MAGNETIC REYNOLDS NUMBER

I. Introduction

Over the past two decades, a number of laboratories have carried out magnetic flux-compression experiments using imploding conducting liners.¹⁻⁷ The liners are cylindrical and surround flux lines parallel to the axis of symmetry. The axial flux may be accompanied by a gas or plasma fill; in some experiments the latter constitutes most of the payload (i.e., supplies most of the pressure opposing the liner implosion), while the magnetic field serves only to reduce thermal losses or as a diagnostic.

The liners have been formed of metal in either solid or liquid state. Chemical explosives,^{1,2} electromagnetic acceleration in the form of θ -pinch^{3,6} and Z-pinch⁴⁻⁶ drives, and hydraulic compression⁷ have been used to implode the liner. With these three driving agencies are associated typical liner velocities v_L of order 10^6 cm/sec, 10^5 cm/sec and 10^4 cm/sec ("fast", "intermediate", and "slow" liners), respectively. (These velocities scale roughly as $v_L \sim (E_D/\rho_L)^{1/2}$, where E_D is the energy density in the drive and ρ_L is the liner mass density.)

A limit on the value of the field strength B which can be obtained is imposed by diffusion of flux from the compression volume, owing to the finite conductivity of the liner. If the liner is given an energy per unit length W_L/ℓ and all of this goes into flux compression, then

$$W_L/\ell \approx \pi r^2 B^2 / 2\mu_0,$$

Note: Manuscript submitted May 26, 1977.

where r is the final compression radius. A skin depth Δ is associated with the diffusion of flux lines into the liner over a time t according to $\Delta^2 = \kappa_o t$, where $\kappa_o = 1/\sigma_o \mu_o$ is the diffusivity, σ_o is the electrical conductivity, μ_o is the (free space) magnetic permeability, and $t \approx r/v_L$ is the time scale of the liner motion. The condition that the flux which leaks out be less than that inside the compression volume is roughly

$$\frac{2\pi r \Delta}{\pi r^2} = 2 \sqrt{\frac{\kappa_o t}{r}} < 1. \quad (2)$$

This is simply a requirement that the magnetic Reynolds number R_m , defined by

$$Re = \frac{r^2}{4\kappa_o t} \quad (3)$$

be greater than unity. For a conductivity equal to that of liquid copper, Eqs. (1) and (2) imply

$$B < 17 (W_L/\ell)^{1/2} v_L, \quad (4)$$

where B is in MG, W_L/ℓ in MJ/m, and v_L is mm/ μ sec.

In the present paper we describe several calculations intended to elucidate the roles of (i) convergence (thickening) of a cylindrical liner and (ii) the detailed time dependence of liner trajectories in the diffusion of magnetic flux into a metal liner. These calculations have been carried out in support of the NRL Linus^{7,8} experiments, in

which a rotating liquid metal liner is imploded hydraulically onto a mixture of plasma and magnetic flux. Ideally, nearly all of the compressional energy should go into the plasma, thereby heating it to kilovolt temperature and initiating thermonuclear reactions, and the magnetic field should be restricted to a thin buffer layer between the plasma and the liner. Maintenance of this layer for the duration of the burn is, of course, essential to containment. Even if only a small portion diffuses into the liner, the Joule heat produced by the penetration of current into the liner can vaporize the latter and release high Z impurities into the plasma. Therefore, a reliable quantitative theory of the diffusion is necessary.

In current and near-term experiments, however, much or all of the "payload" consists of magnetic flux. In this paper we therefore simplify our problem by ignoring the plasma entirely. We also ignore field line fringing and curvature so as to make the problem one-dimensional. (This is strictly correct at the midplane of the experimental device, if nowhere else.)

Within the limitations thus invoked, our objective is to calculate in detail how much flux leaks out of the compression region, retaining realistic conductivities, liner trajectories, and the associated liner convergence. Previous work⁹ has, for the most part, been restricted to slab geometry, using a vacuum magnetic field prescribed on the basis of analytical convenience rather than consistency with realistic trajectories.

Below in Section II we develop a formalism applicable to either slab or cylindrical liners. A detailed treatment of the former is presented in the Appendix to facilitate reference and comparison with the cylindrical case. In Section III we specialize to the limit of greatest interest, the weak-diffusion (high magnetic Reynolds number) limit, and solve the resulting boundary layer problem. The calculation of total diffused flux, magnetic energy in the liner and Joule heat is reduced to a series of quadratures with respect to the trajectory. The diffused flux per unit surface area is precisely the same as in the slab problem. In other words, the flux diffusion rate is proportional to the instantaneous radius. Therefore the total diffused flux is proportional to an average radius, whose value depends on the details of the liner trajectory. Section IV describes the results of applying this formalism to two prescribed model trajectories, termed "sinusoidal" and "parabolic." We conclude in Section V with a brief discussion of the results.

II. Derivation of the Formalism

Consider a situation in which a cylindrical vacuum region of radius R_1 contains a uniform axial magnetic field (see Fig. 1). The material surrounding the vacuum (the liner) is assumed to be incompressible, extends to infinity and has a finite electrical conductivity σ . R_1 may be a function of time, in which case there is a radial flow field within the medium. It is assumed that at $t = 0$ the magnetic field vanishes outside the vacuum region. Its subsequent evolution is determined by Ampère's law

$$\nabla \times \underline{B} = \mu \underline{J} , \quad (5)$$

Faraday's law

$$\frac{\partial \underline{B}}{\partial t} = - \nabla \times \underline{E} , \quad (6)$$

and Ohm's law

$$\sigma [\underline{E} + \underline{v} \times \underline{B}] = \underline{J} , \quad (7)$$

where \underline{v} is the velocity field. With the assumptions of one-dimensionality, incompressibility and straight field lines, Eqs. (5-7) yield the convective diffusion equation

$$\frac{\partial B}{\partial t} + v \frac{\partial B}{\partial r} = \frac{1}{r^{\delta-1}} \frac{\partial}{\partial r} (\kappa r^{\delta-1} \frac{\partial B}{\partial r}), \quad (8)$$

where $\delta = 1, 2$ for slab, cylindrical geometry, respectively, and κ is the diffusivity, defined by

$$\kappa = 1/\mu\sigma \quad . \quad (9)$$

In general κ depends on position explicitly or through the temperature dependence of σ , and we can write

$$\kappa = \kappa_0 F \quad . \quad (10)$$

Here κ_0 is a constant indicative of the scale of κ and F is a dimensionless quantity which can depend on r and the history of B .

Corresponding to Eq. (8) the initial condition is

$$B(r, 0) = 0, \quad r > R_1(0) \quad , \quad (11)$$

and the boundary conditions are

$$\lim_{r \rightarrow \infty} B(r, t) = 0 \quad ; \quad (12)$$

$$B_1(t)R_1^\delta(t) + \delta \int_{R_1}^{\infty} dr r^{\delta-1} B(r, t) = B_1(0)R_1^\delta(0) \quad . \quad (13)$$

Equation (13) is the expression of conservation of total magnetic flux. These boundary conditions correspond to an initially field-free liner. The case where there is a non-vanishing field profile within the liner initially can also be treated, and the results can be related to those of the present case. For large compression ratios (see Section IV), the effect of the initial profile is negligible.

It is convenient to scale $B(r,t)$ by the maximum value of the vacuum field associated with the implosion, B_0 :

$$b = B(r,t)/B_0, \quad (14)$$

and to scale t by a time t_0 , characteristic of the liner motion,

$$\tau = t/t_0. \quad (15)$$

Equation (8), which represents the Eulerian form of the convective-diffusion equation, is not in the most advantageous form to calculate the diffusion into a moving liner. This is because the boundary condition of total flux conservation, Eq. (13), is applied at the moving boundary, $R_1(t)$. Furthermore there are really two time scales associated with Eq. (8): the convective time scale, $\dot{R}_1/R_1(t)$, and the diffusive time scale, κ_0/R_1^2 . It is most useful to cast Eq. (8) in Lagrangian form. For the incompressible liners considered here the Lagrangian variable is

$$\xi = (r^\delta - R_1^\delta)/R_0^\delta. \quad (16)$$

where R_0 is the minimum radius. The system of equations now becomes

$$\frac{\partial b}{\partial \tau} = R_m^{-1} \frac{\partial}{\partial \xi} \left\{ F[\bar{R}_1^\delta + \xi] \frac{2(\delta-1)}{\delta} \frac{\partial b}{\partial \xi} \right\}; \quad (17)$$

$$b(\xi, 0) = 0, \quad \xi > 0; \quad (18)$$

$$\lim_{\xi \rightarrow \infty} b(\xi, \tau) = 0; \quad (19)$$

$$b_1(\tau) \bar{R}_1^\delta + \int_0^\infty d\xi b(\xi, \tau) = 1, \quad (20)$$

where $b_1(\tau) = b(0, \tau) = B_1/B_0$, the scaled liner radius R_1/R_0 is denoted by \bar{R}_1 , and the magnetic Reynolds number Rm is defined by

$$Rm = R_0^2 / \delta^2 \mu_0 t_0 \quad (21)$$

The slab case, shown in Fig. 2, is treated in the Appendix. Equations (17-20) with $\delta = 3$ (spherical geometry) apply to such processes as heat diffusion from a collapsing reservoir, but not to magnetic flux diffusion. Spherical (or quasispherical) flux surfaces not only do not arise even in three-dimensional implosions, they also contradict the assumption of straight field lines employed in the derivation of Eq. (8). Thus in the body of this paper we restrict ourselves to the cylindrical case, $\delta = 2$, and rewrite the equations accordingly. The Lagrangian spatial variable is then from Eq. (16)

$$\xi = (r^2 - R_1^2) / R_0^2, \quad (22)$$

and the appropriate form of the equations is

$$\frac{\partial b}{\partial \tau} = Rm^{-1} \frac{\partial}{\partial \xi} [(\bar{R}_1^2 + \xi) \frac{\partial b}{\partial \xi}]; \quad (23)$$

$$b(\xi, 0) = 0, \quad \xi > 0; \quad (24)$$

$$\lim_{\xi \rightarrow \infty} b(\xi, \tau) = 0; \quad (25)$$

$$b_1(\tau) \bar{R}_1^2 + \int_0^\infty d\xi b(\xi, \tau) = 1, \quad (26)$$

with

$$Rm = R_0^2 / 4 \kappa_0 t_0. \quad (27)$$

Some results of an approximate nature can be found when $Rm = 0$ (static liner). Given b_1 , the value of b at $r = R_1$, the solution for the diffusion of b outward from the surface $r = R_1$ into a region where $b = 0$ initially is well-known¹⁰:

$$b(\rho, \tau) = \frac{2}{\pi} \int_0^\tau d\tau' b_1(\tau') \int_0^\infty du u e^{-u^2(\tau-\tau')} \quad (28)$$

$$\frac{J_0(u) Y_0(\rho u) - J_0(\rho u) Y_0(u)}{J_0^2(u) + Y_0^2(u)},$$

where $\rho = r/R_1$. Substitution into Eq. (26) yields an integral equation for b_1 ,

$$b_1(\tau) + \left(\frac{2}{\pi}\right)^2 \int_0^\tau d\tau' b_1(\tau-\tau') \int_0^\infty \frac{du e^{-u^2\tau}}{u[J_0^2(u) + Y_0^2(u)]} = 1 \quad (29)$$

For small τ , $b_1 \approx 1$, and the lowest order correction can be found by iteration, using the asymptotic expansion for the Bessel functions J_0 and Y_0 :

$$b_1(\tau) \approx 1 - \left(\frac{2}{\pi}\right)^2 \int_0^\tau d\tau' \int_0^\infty \frac{du e^{-u^2\tau'}}{u[J_0^2(u) + Y_0^2(u)]} \quad (30)$$

$$\approx 1 - \frac{2\tau}{\sqrt{\pi}}$$

Analogously, for $\tau \rightarrow \infty$ the small-argument expansion of the Bessel functions leads in lowest order to

$$b_1(\tau) \sim \frac{1}{\tau \ln \tau} \quad . \quad (31)$$

We note that $b_1(\tau) \rightarrow 0$ faster than in the slab case (see Appendix), in accord with the intuitive notion that radial efflux is less constrained than is rectilinear efflux.

III. Large Magnetic Reynolds Number

The case of chief experimental interest is that of large magnetic Reynolds number,

$$R_m = R_0^2 / 4\mu_0 t_0 \gg 1, \quad (32)$$

since this is the limit of efficient compression. Now the situation is greatly simplified. We anticipate that diffusive effects should be localized in a very thin boundary layer near the liner-vacuum interface. That is, the magnetic flux distribution should differ only by a small perturbation from that for an ideal adiabatically compressed trapped flux.

To establish this result rigorously, we proceed using the methods of matched asymptotic analysis. The relevant equations are Eq. (23), the Lagrangian form of the convective-diffusion equation, with initial conditions given by Eq. (24) and boundary conditions given by Eqs. (25) and (26). It is assumed in the analysis that the form factor F remains of order unity. We identify and treat separately two regions, as follows.

Outer Region

We assume a regular perturbation expansion for the scaled magnetic field strength b in powers of the small parameter $R_m^{-1/2}$,

$$\begin{aligned} b(\xi, \tau; \epsilon; R_m) = & b^{(0)}(\xi, \tau; \epsilon) + R_m^{-1/2} b^{(1)}(\xi, \tau; \epsilon) \\ & + R_m^{-1} b^{(2)}(\xi, \tau; \epsilon) + \dots \end{aligned} \quad (33)$$

To lowest order in $Rm^{-1/2}$ we find from Eqs. (23-26)

$$\frac{\partial b^{(0)}}{\partial \tau} = 0 ; \quad (34)$$

$$b^{(0)}(\xi, 0) = 0, \quad \xi > 0; \quad (35)$$

$$\lim_{\xi \rightarrow \infty} b^{(0)}(0, \tau) = 0; \quad (36)$$

$$b^{(0)}(0, \tau) = b_1(\tau) = \bar{R}_1^{-2}. \quad (37)$$

The solution of Eq. (34) which satisfies conditions (35) and (36) is

$$b^{(0)}(\xi, \tau) = 0. \quad (38)$$

However, this solution does not satisfy the second boundary condition, Eq. (37). We thus have the ingredients for a classical boundary layer. It is necessary to rescale the independent variable ξ to recover the missing boundary condition and resolve this layer.

Inner Region

The rescaling is performed by defining

$$\eta = Rm^{1/2} \xi. \quad (39)$$

When Eq. (39) is introduced in Eqs. (23-26) we obtain

$$\frac{\partial b}{\partial \tau} = \frac{\partial}{\partial \eta} [F(\bar{R}_1^2(\tau) + Rm^{-1/2} \eta) \frac{\partial b}{\partial \eta}] ; \quad (40)$$

$$b(\eta, 0) = 0 ; \quad (41)$$

$$\lim_{\eta \rightarrow \infty} b(\eta, \tau) = 0 ; \quad (42)$$

$$b(0, \tau) \bar{R}_1^2 + Rm^{-1/2} \int_0^\infty d\eta b(\eta, \tau) = 1. \quad (43)$$

Again expanding as in Eq. (33) yields in lowest order

$$\frac{\partial b^{(0)}}{\partial \tau} = \bar{R}_1^2 \frac{\partial}{\partial \eta} \left(F \frac{\partial b^{(0)}}{\partial \eta} \right) ; \quad (44)$$

$$b^{(0)}(\eta, 0) = 0 ; \quad (45)$$

$$\lim_{\eta \rightarrow \infty} b^{(0)}(\eta, \tau) = 0 ; \quad (46)$$

$$b^{(0)}(0, \tau) = b_1(\tau) = \bar{R}_1^{-2} . \quad (47)$$

This is just the condition for adiabatic flux compression.

If we define a new timelike variable, the "age"

$$\theta = \int_0^\tau \bar{R}_1^2(\tau') d\tau' , \quad (48)$$

Eq. (44) simplifies to a slab-type diffusion equation,

$$\frac{\partial b^{(0)}}{\partial \theta} = \frac{\partial}{\partial \eta} \left(F \frac{\partial b^{(0)}}{\partial \eta} \right) . \quad (49)$$

Equation (49) embodies both the cylindrical geometry and the liner motion in a relation which is formally identical with that obtained

in planar geometry. Thus for $Rm \gg 1$, any calculation which can be done in slab geometry can be carried over to the cylindrical case.

If at this point we rule out the possibility of thermal, etc., variation of σ and set

$$F = 1,$$

we can use the results derived in the Appendix to write down the diffused magnetic field,

$$B(\eta, \theta) = \frac{2B_0}{\sqrt{\pi}} \int_{\eta/2\sqrt{\theta}}^{\infty} ds e^{-s^2} b_1(\tau - \eta^2/4s^2), \quad (50)$$

where b_1 is given by Eq. (47). From Eq. (50) we find the total diffused flux,

$$\begin{aligned} \Phi &= 2\pi \int_{R_1}^{\infty} r dr B(r, \tau) \\ &= \frac{\sqrt{\pi} B_0 R_0^2}{Rm^{1/2}} \int_0^{\theta} d\theta' \frac{b_1(\theta')}{\sqrt{\theta - \theta'}}; \end{aligned} \quad (51)$$

the total magnetic energy,

$$\begin{aligned} W_M &= 2\pi \int_{R_1}^{\infty} r dr \frac{B^2(r, \tau)}{2\mu} \\ &= \frac{\pi^{3/2} B_0^2 R_0^2}{4 Rm^{1/2}} \int_0^{\theta} d\theta' \int_0^{\theta} d\theta'' \frac{b_1(\theta') b_1(\theta'')}{\sqrt{2\theta - \theta' - \theta''}}, \end{aligned} \quad (52)$$

and the total Joule heat,

$$W_T = - \frac{\pi^{3/2}}{2} \frac{B_0^2 R_0^2}{Rm^{1/2}} \int_0^\infty d\theta' b_1(\theta') \quad (53)$$

$$\left[\frac{1}{\sqrt{\theta}} + \int_0^{\theta'} d\theta'' \frac{\partial b_1 / \partial \theta''}{(\theta' - \theta'')^{1/2}} \right] = W_M.$$

Equations (50-53) correctly determine Φ , W_M and W_T for any form of the vacuum field $B_1(t)$, even if Eq. (47), the condition for adiabatic flux compression, is not satisfied. In the present instance, $b_1(\theta) = [\bar{R}_1(\theta)]^{-2}$ and therefore the liner field, diffused flux, and magnetic and thermal energy distributions are seen to be given as quadratures over the liner trajectory, $R_1(\tau)$, in this large Reynolds number limit. Now all that remains is to supply the trajectory $R_1(\tau)$. In general $R_1(\tau)$ must be obtained by considering all the forces acting on the liner. To emphasize the physics of the problem in its most simple form, we will instead consider the radial trajectory to be prescribed and generate solutions consistent with this trajectory.

IV. Numerical Results

We wish to apply the preceding results to trajectories which are symmetric, smooth and contain the compression ratio α (initial radius divided by final radius) as a parameter. Two examples are the sinusoidal trajectory,

$$R_0^2/R_1^2(t) = \epsilon + (1-\epsilon) \sin(\pi t/2t_0), \quad (54)$$

and the parabolic trajectory,

$$R_1^2(t)/R_0^2 = 1 + (\epsilon^{-1} - 1)(1-t/t_0)^2. \quad (55)$$

In both of these $R_1 = R_0$, the minimum radius, when $t = t_0$, and $R_1(0) = \epsilon^{-1/2} R_0$, i.e., $\alpha = \epsilon^{-1/2}$.

But there is an essential difference. For the sinusoidal model, $\dot{R}_1 t_0 / R_1 \approx -\pi/4\epsilon \gg 1$ at $t = 0$, while in the parabolic model, $\dot{R}_1 t_0 / R_1 \approx -1$. Consequently, the typical value of the normalized vacuum field b_1 in the former case is close to unity and nearly independent of ϵ , since the liner spends comparatively little time at large radii (see Fig. 3). This is reflected in the age variable θ . This tends to be much smaller in the sinusoidal case, but the sinusoidal trajectory spends a greater age in the vicinity of turnaround, where the driving field is near its maximum value.

When we use Eq. (51) to evaluate the diffused flux Φ as a function of time for these cases, we obtain the results shown in Fig. 4. We expect the sinusoidal trajectory to be more lossy. This is seen to be true, except at $t \approx 2t_0$. Diffused flux

leaks back into the vacuum region when the vacuum field drops below the values in the liner. Since the flux has not gotten very far into the liner in the sinusoidal case, it leaks back out very quickly. In contrast, the "older" parabolic trajectories cannot empty all the flux back into the vacuum region, even though the driving field drops away more abruptly after turnaround. Note that in all cases, this return diffusion does not begin until $\left. \frac{\partial B}{\partial \eta} \right|_{\eta=0} = 0$ (c.f. Eq. A8), i.e., somewhat after turnaround.

To display the dependence of our results on the trajectory and the vacuum magnetic field, we proceed as follows. The diffused flux for a constant vacuum field is obtained by writing $b_1 = 1$ in Eq. (51):

$$\Phi(\theta) = \frac{\sqrt{\pi} B_0 R_0^2}{R_m^{1/2}} \int_0^\theta d\theta' (\theta - \theta')^{-1/2} = \frac{2\sqrt{\pi} B_0 R_0^2}{R_m^{1/2}} \theta^{1/2}. \quad (56)$$

Substituting for R_m from Eq. (27), we have

$$\Phi(t) = 2\pi \langle R_1^2 \rangle^{1/2} B_0 (4\pi t/\pi)^{1/2}, \quad (57)$$

where

$$\langle R_1^2 \rangle = \frac{1}{t} \int_0^t dt' R_1^2(t') \quad (58)$$

is the mean square of the liner radius as a function of time. Thus the trajectory enters only through the factor $\langle R_1^2 \rangle^{1/2}$. In the general case, when b_1 also depends on time, either through Eq. (47) or otherwise, we can write

$$\Phi(t) = 2 \pi \langle R_1^2 \rangle^{1/2} \langle B_1 \rangle (4\kappa t/\pi)^{1/2}, \quad (59)$$

where $\langle B_1 \rangle$ is a shape factor, representing some time average of the driving field. As a rule, the product $\langle R_1^2 \rangle^{1/2} \langle B_1 \rangle$ can only be obtained by numerical evaluation of Eq. (51).

To make contact with the results of Knoepfel⁹, we consider three cases: (a) the sinusoidal model [Eq. (54)] with $\epsilon = 1$, i.e., $B_1 = B_0 = \text{constant}$ and $R_1 = R_0 = \text{constant}$; (b) the $\epsilon = 0.001$ sinusoidal case described above; and (c) a static liner with $R_1 = R_0$ but $B/B_0 = \sin(\pi t/2t_0)$ [i.e., the field which would result from letting $\epsilon \rightarrow 0$ in Eq. (54)]. The corresponding diffused fluxes are plotted against time in Fig. 5. Curve (a), which increases without bound, is just found by writing $\langle R_1^2 \rangle = R_0^2$ in Eq. (57). The result is the same as that of Knoepfel for the constant vacuum field case. Curve (b) is identical with the upper trace in Fig. 4. Curve (c) is found by replacing θ with $\tau = t/t_0$ in Eq. (51). (The difference between $\epsilon = 0.0$ and $\epsilon = 0.001$ is undetectable on the scale of the plot).

We can define a flux skin depth in the usual fashion as

$$s_\phi = \Phi(t)/2\pi R_0 B_0. \quad (60)$$

Substituting Φ from Eq. (59) we obtain

$$s_\phi = \sqrt{4/\pi} (\langle R_1^2 \rangle^{1/2}/R_0) (\langle B_1 \rangle/B_0) \sqrt{\kappa t} \quad (61)$$

where $\sqrt{4/\pi} = 1.128$ is recognized as Knoepfel's⁹ coefficient for slab diffusion with a constant driving field. In a similar fashion, skin

depths may be defined for magnetic energy (s_M), joule energy (s_T), and total energy (s_E). In Table I these skin depths at $t = t_0$ are tabulated and compared to Knoepfel's values (Ref. 9, p.77) for a sinusoidal driving field on a slab liner.

Figure 6 shows plots of the thermal and magnetic energy of diffusion associated with the trajectories of Fig. 3. Since the energies are quadratic in B, the enhanced losses obtained with the flatter sinusoidal trajectories are more pronounced here.

For overall energetic consideration, two measures of the losses associated with flux diffusion are particularly useful (Fig. 7). These are the total ($W_M + W_T$) energy loss at turnaround, divided by the payload energy $W_0 = \pi R_0^2 B_0^2 / 2\mu_0$ and the thermal energy W_T at return divided by W_0 . The first tells how much the finite conductivity affects the maximum compression, while the second measures the tendency of the liner not to rebound exactly, as well as the amount of heat it absorbs per cycle.

Finally, for some applications a detailed knowledge of the diffused flux profile is needed. Figure 8 shows how such profiles evolve for a particular case. Note that the picture of a thin layer near the boundary is weakest near turnaround. The variable η , of course, measures area, not displacement. Even though the trace for $t = 2.0$ is broader than the earlier ones, the thickness of the layer

$$\Delta \sim \frac{1}{2} \langle \eta \rangle R_m^{-1/2} R_0^2 / R_1 ,$$

where $\langle \eta \rangle$ is an average or typical value of η for the profile, evidently drops rapidly after turnaround.

V. Conclusion

The principal result of this paper has been the establishment of a simple procedure to handle diffusion problems in imploding cylindrical systems at large Reynolds number. The particular application treated here, flux diffusion in imploding cylindrical axial flux compression devices, has emphasized the boundary layer character of this problem.

If the equations are cast in Lagrangian variables, the large Reynolds number limit leads to a "slab"-like system of equations if the time variable is suitably weighted over the implosion trajectory. To lowest order in $Rm^{-1/2}$, the magnetic flux payload is compressed adiabatically (supplying the boundary condition for the magnetic diffusion problem). The diffused flux and magnetic and thermal energies are all confined near the compression surface within a boundary layer whose depth is of order $Rm^{-1/2}$.

The main aspects of this approach are also valid in other problems involving the diffusion of a scalar quantity into a moving medium at large associated Reynolds numbers, that is, wherever the hydrodynamic time scale dictated by the basic system motion is short compared to the relevant diffusive time scale. The same procedure can treat slab, cylindrical, and spherical diffusion problems in this limit.

Acknowledgment

We wish to thank Dr. A. E. Robson for his interest and encouragement. This work was supported by the Office of Naval Research and the U.S. Energy Research and Development Administration.

Appendix: The Convection-Diffusion Problem in Slab Geometry

As might be expected, the planar analog of the problem of flux diffusion into a cylindrical liner is relatively tractable and affords a convenient means of understanding the principal physical features of the latter. Now the vacuum region is located between a perfectly conducting wall at $x = 0$ and a moving liner-vacuum interface at $x = x_1$ (see Fig. 2). Equations (16-21) become

$$\xi = (x - x_1)/x_0; \quad (A1)$$

$$\frac{\partial b}{\partial \tau} = \text{Rm}^{-1} \frac{\partial^2 b}{\partial \xi^2}; \quad (A2)$$

$$b(\xi, 0) = 0, \quad \xi > 0; \quad (A3)$$

$$\lim_{\xi \rightarrow \infty} b(\xi, \tau) = 0; \quad (A4)$$

$$b_1 x_1 / x_0 + \int_0^{\infty} d\xi \, b(\xi, \tau) = 1, \quad (A5)$$

with $x_0 = x_1(0)$ and

$$\text{Rm} = x_0^2 / \nu_0 t_0. \quad (A6)$$

If $b_1(\tau)$ were known, the solution of Eqs. (A2-A4) could be written down immediately using standard results from diffusion theory.¹⁰

$$b(\eta, \tau) = \frac{2}{\sqrt{\pi}} \int_{\frac{\eta}{2\sqrt{\tau}}}^{\infty} ds e^{-s^2} b_1\left(\tau - \frac{\eta^2}{4s^2}\right), \quad (A7)$$

where ξ has been replaced by the stretched variable

$$\eta = \xi Rm^{1/2}. \quad (A8)$$

Because of the non-standard boundary condition Eq. (A5), however, b_1 is not known, and self-consistent solutions for finite Rm in general require numerical techniques.

Some of the analysis can be carried out in closed form, however, in the case of uniform motion,

$$x_1(\tau) = x_0 + V_0 \tau = V_0(\tau \pm \tau_0), \quad (A9)$$

where $\tau_0 = x_0/|V_0|$. Substituting (A7) into (A5) yields

$$b_1(\sigma)(1 + \omega\sigma) + \frac{1}{\sqrt{\pi}} \int_0^\sigma \frac{d\sigma' b_1(\sigma')}{\sqrt{\sigma - \sigma'}} = 1, \quad (A10)$$

where

$$\omega = \pm Rm^{-1}, \quad (A11)$$

the sign depending on that of V_0 , and

$$\sigma = \tau Rm, \quad (A12)$$

with τ defined by Eq. (15).

The Abel equation (A10) can be solved by Laplace transforms, provided $\omega > 0$. Define

$$a(s) = \int_0^{\infty} d\sigma e^{-s\sigma} b_1(\sigma). \quad (13)$$

Then

$$a(1 + s^{-1/2}) + \omega \frac{da}{ds} = s^{-1}, \quad (A14)$$

whence

$$a(s) = \frac{2}{\omega} \int_1^{\infty} \frac{d\lambda}{\lambda} \exp \left[- \frac{s(\lambda^2 - 1) + 2\sqrt{s}(\lambda - 1)}{\omega} \right]. \quad (A15)$$

Inversion of (A15) leads to

$$b_1(\sigma) = \frac{2}{\sqrt{\pi} \omega^2} \int_1^{\sqrt{1+\omega\sigma}} \frac{d\lambda}{\lambda} \frac{\lambda - 1}{(\sigma + \frac{1-\lambda^2}{\omega})} \exp \left[\frac{-(\lambda - 1)^2/\omega^2}{\sigma + \frac{1-\lambda^2}{\omega}} \right]. \quad (A16)$$

Next we note (by direct substitution if necessary) that the solution (A16) works equally well for $\omega < 0$, provided $1 + \omega\sigma > 0$. Finally we reintroduce τ and Rm explicitly, rewriting the integral in the process to obtain

$$b_1(\tau) = \frac{2}{\sqrt{-\pi\omega}} \int_0^{\infty} dz e^{+\frac{z^2}{\omega}} \frac{z(1-z^2)}{\sqrt{1+(1+\omega\tau)(z^2-1)} [1 - z\sqrt{1+(1+\omega\tau)(z^2-1)}]} \quad (A17)$$

a form which is only valid for $\omega < 0$.

Though unwieldy, this result provides some useful information.

First, the limit $\omega \rightarrow 0$ yields the static liner result

$$b_1(\tau) = e^\tau \operatorname{erfc}(\sqrt{\tau}) \quad (\text{A18})$$

where erfc denotes the complimentary error function. For $\tau \rightarrow \infty$, the asymptotic form of the latter leads to

$$b_1(\tau) \sim \frac{1}{\sqrt{\pi\tau}}. \quad (\text{A19})$$

Secondly, when $1 + \omega\tau = 0$ (totally imploded liner), Eq. (A17) reduces to

$$\begin{aligned} b_1(-\omega^{-1}) &= 2\sqrt{\frac{\tau}{\pi}} \int_0^\infty dz e^{-\tau z^2} z(1+z) \\ &= \frac{1}{\sqrt{\pi\tau}} \left(1 + \frac{1}{2}\sqrt{\frac{\pi}{\tau}}\right). \end{aligned} \quad (\text{A20})$$

Thus the vacuum field strength remains finite no matter how rapid the compression; indeed, if R_m is less than a critical value \tilde{R}_m given by

$$\tilde{R}_m = \frac{1}{2} \left[1 + \frac{1}{\pi} (1 + \sqrt{1 + 2\pi})\right] \approx 1.09 \quad (\text{A21})$$

b_1 decreases monotonically. Lastly, for $\omega \gg 1$ (the large magnetic Reynolds number limit),

$$b_1(\tau) \rightarrow \frac{1}{1+\omega\tau} = x_0/x_1. \quad (\text{A22})$$

Corrections to the lowest order result are evidently $\sim \text{Rm}^{-1/2}$ and may be calculated systematically.

In the limit $\text{Rm} \gg 1$, however, Eq. (A5) reduces to $b_1(\tau) = x_0/x_1$, independent of any ansatz of the form (A9). Given a knowledge of the trajectory $x_1(\tau)$, all of the quantities of physical interest can be found from (A7). Thus the total flux diffused into the liner is

$$\Phi = \int_{x_1}^{\infty} dx B(x, t) \approx \frac{B_0 x_0}{(\pi \text{Rm})^{1/2}} \int_0^{\tau} d\tau' \frac{b_1(\tau')}{\sqrt{\tau - \tau'}}. \quad (\text{A23})$$

The rate of change of Φ with time is given by

$$\frac{\text{Rm}^{1/2}}{B_0 x_0} \frac{d\Phi}{d\tau} = \int_0^{\infty} d\eta \frac{\partial b}{\partial \tau} = \int_0^{\infty} d\eta \frac{\partial^2 b}{\partial \eta^2} = - \left. \frac{\partial b}{\partial \eta} \right|_{\eta=0} \quad (\text{A24})$$

Hence from (A3),

$$\begin{aligned} \lim_{\eta \rightarrow 0+} \frac{\partial b}{\partial \eta} &= - \frac{1}{\sqrt{\pi}} \frac{\partial}{\partial \tau} \int_0^{\tau} d\tau' \frac{b_1(\tau')}{\sqrt{\tau - \tau'}} \\ &= - \frac{b_1(0)}{\sqrt{\pi \tau}} - \frac{1}{\sqrt{\pi}} \int_0^{\tau} d\tau' \frac{\partial b_1 / \partial \tau'}{(\tau - \tau')^{1/2}} \end{aligned} \quad (\text{A25})$$

The magnetic energy associated with the diffused flux is

$$\begin{aligned}
W_M &= \frac{x_o B_o^2}{2\mu_o Rm^{1/2}} \int_0^\infty d\eta \, b^2(\eta, \tau) \\
&= \frac{B_o^2 x_o}{4\mu_o} \left(\frac{\pi}{Rm} \right)^{1/2} \int_0^\tau d\tau' \int_0^\tau d\tau'' \frac{b_1(\tau') b_1(\tau'')}{\sqrt{2\tau - \tau' - \tau''}}
\end{aligned} \tag{A26}$$

after an interchange in orders of integration. The Joule heat is

$$\begin{aligned}
W_T &= \int_0^\tau d\tau' P_T(\tau') \\
&= \frac{x_o B_o^2}{\mu_o} \left(\frac{\pi}{Rm} \right)^{1/2} \int_0^\tau d\tau' \int_0^\infty d\eta \left(\frac{\partial b}{\partial \eta} \right)^2.
\end{aligned} \tag{A27}$$

The interchange of orders of integration is not valid here. Instead we integrate by parts, using (A25):

$$\begin{aligned}
W_T &= - \frac{x_o B_o^2}{\mu_o} \left(\frac{\pi}{Rm} \right)^{1/2} \int_0^\tau d\tau' \left[b_1(0, \tau') \frac{\partial b(0, \tau')}{\partial \eta} - \int_0^\infty d\eta \, b_1 \frac{\partial b_1}{\partial \tau'} \right] \\
&= \frac{x_o B_o^2}{\mu_o} \left(\frac{\pi}{Rm} \right)^{1/2} \int_0^\tau d\tau' b_1(\tau') \left[\frac{1}{\sqrt{\tau'}} + \int_0^\tau d\tau'' \frac{\partial b_1 / \partial \tau'}{(\tau - \tau'')^{1/2}} \right] - W_M.
\end{aligned} \tag{A28}$$

Although (A26) and (A27) are manifestly positive, (A28) is not.

Nonetheless, numerical evaluations of (A26) and (A28) reveals that

$W_T \geq W_M$, a relation which can be shown to hold in general.

References

1. C. M. Fowler, W. B. Garn and R. S. Caird, J. Appl. Phys. 31, 588 (1960).
2. A. D. Sakharov, R. Z. Lyudaev, E. N. Smirnov, Yu. I. Plyushchev, A. J. Pavlovskii, V. K. Chernyshev, E. A. Feoktistova, E. J. Zharinov, and Yu. A. Zysin, Dokl. Akad. Nauk USSR 165, 65 (1965) [Sov. Phys. - Dokl. 10, 1045 (1966)].
3. E. C. Cnare, J. Appl. Phys. 37, 3812 (1966).
4. S. G. Alikhanov, V. G. Belan, G. J. Budker, , A. J. Ivanchenko and G. N. Kichigin, At. Energ. 23, 536 (1967) [Sov. J. At. Energy 23, 1307 (1967)].
5. J. Besançon, J. Morin and J. Vedel, C. R. Acad. Sci. B267, 1319 (1968).
6. S. G. Alikhanov, V. P. Bakhtin, V. M. Brusnikin, I. S. Glushkov, R. Kh. Kurtmullaev, A. L. Lunin, A. D. Muzychenko, V. P. Novikov, V. V. Pichugin, V. N. Semenov, G. E. Smolkin, E. G. Utyugov and I. Ya. Shipuk, Proc. 6th Int. Conf. on Plasma Physics and Controlled Thermonuclear Fusion Research, Berchtesgaden, FGR, October 1976 (IAEA, Vienna, to be published), paper No. E-19-2.
7. D. L. Book, A. L. Cooper, R. Ford, D. Hammer, D. J. Jenkins, A. E. Robson, P. J. Turchi, Proc. 6th Int. Conf. on Plasma Physics and Controlled Nuclear Fusion Research, Berchtesgaden, FGR, October 1976 (IAEA, Vienna, to be published) paper No. E-19-1.
8. P. J. Turchi, A. L. Cooper, R. Ford, and D. J. Jenkins, Phys. Rev. Lett. 36, 1546 (1976).

9. Heinz Knoepfel, Pulsed High Magnetic Fields (North-Holland Publishing Co., Amsterdam, 1976), Ch. 3.
10. H. S. Carslaw and J. C. Jaeger, Conduction of Heat in Solids, Second Edition (Clarendon Press, Oxford, 1959).

TABLE I SKIN DEPTHS FOR SINUSOIDAL TRAJECTORY: Comparison with
Static Liner and Sinusoidal Field at $t = t_0$

ϵ	Flux $s_\phi / \sqrt{\kappa t}$	Joule $s_T / \sqrt{\kappa t}$	Magnetic $s_M / \sqrt{\kappa t}$	Total $s_E / \sqrt{\kappa t}$
.001	1.065	.684	.582	1.266
.01	1.067	.686	.583	1.270
.15	1.081	.753	.598	1.351
.30	1.092	.856	.611	1.468
.45	1.101	.984	.623	1.606
Slab ^g	.88	.718	.500	1.223

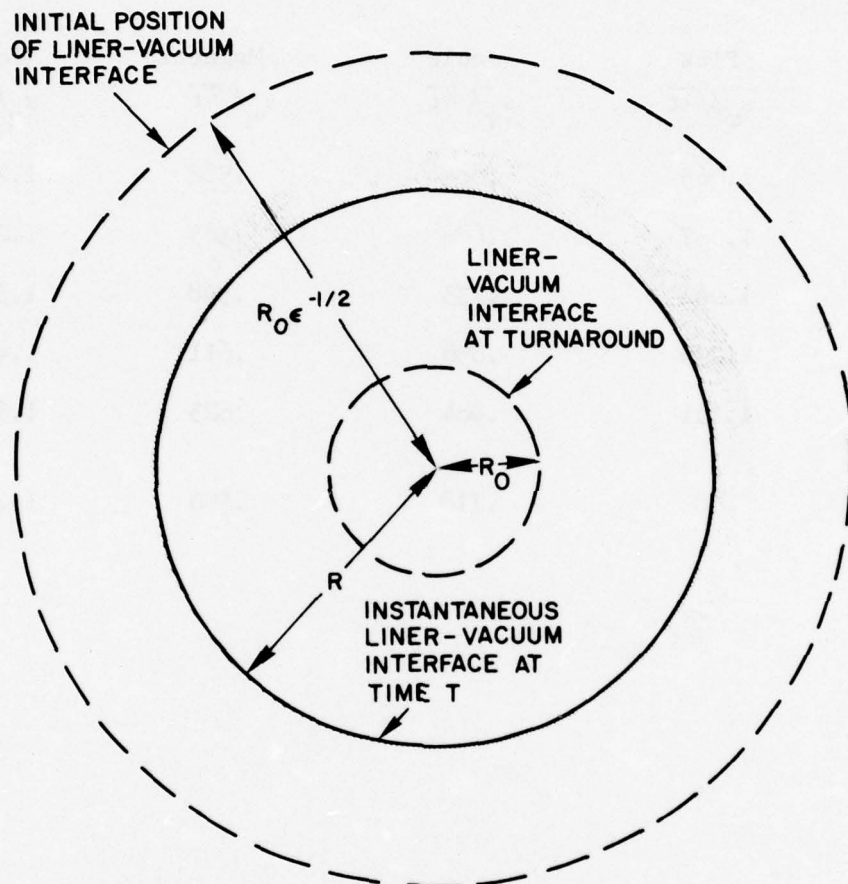


Fig. 1 — Schematic of cylindrical liner compressing an axial flux. The radius of the liner-vacuum interface is $R_1 = R_0 \epsilon^{-1/2}$ at $t = 0$ and $R_1 = R_0$ at turnaround ($t = t_0$). The shaded region represents the layer occupied by diffused flux.

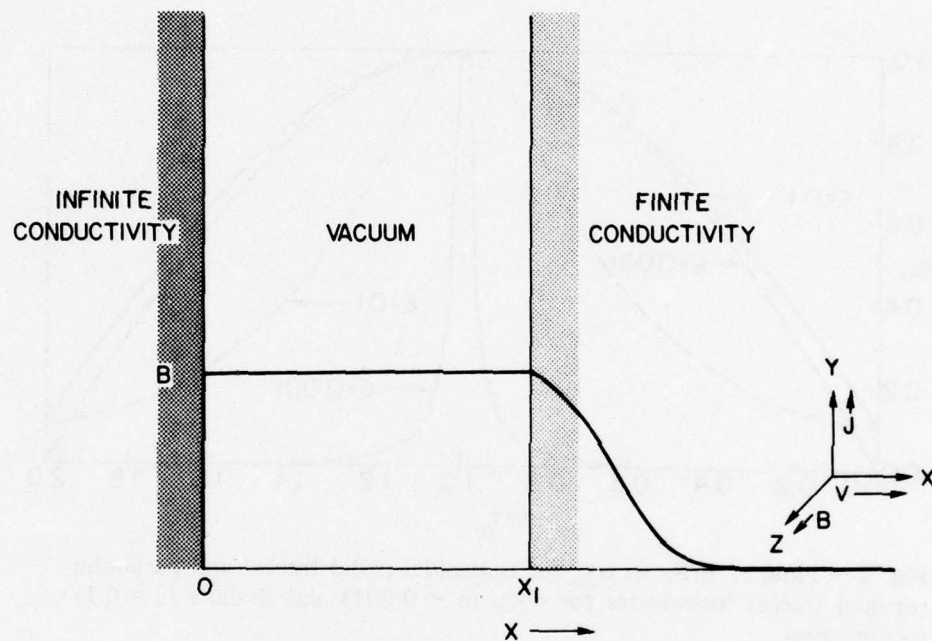


Fig. 2 — Slab equivalent of the model shown in Fig. 1. A region of infinite conductivity lies to the left of $x = 0$. Inside the "liner" (the region of finite σ , $x > x_1$) the field strength falls from its vacuum value to zero.

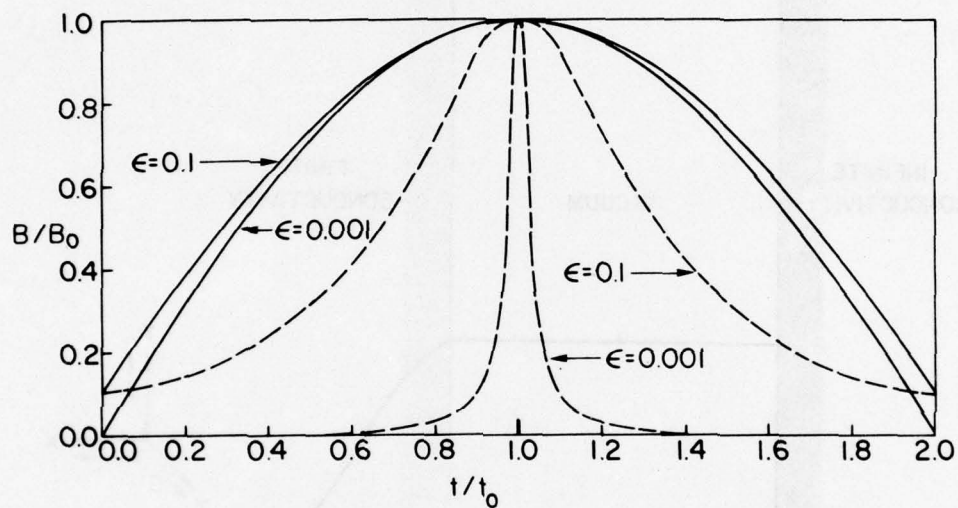


Fig. 3 — Plots of B/B_0 vs t/t_0 for sinusoidal (solid traces) and parabolic (broken traces) trajectories for deep ($\epsilon = 0.001$) and shallow ($\epsilon = 0.1$) compression

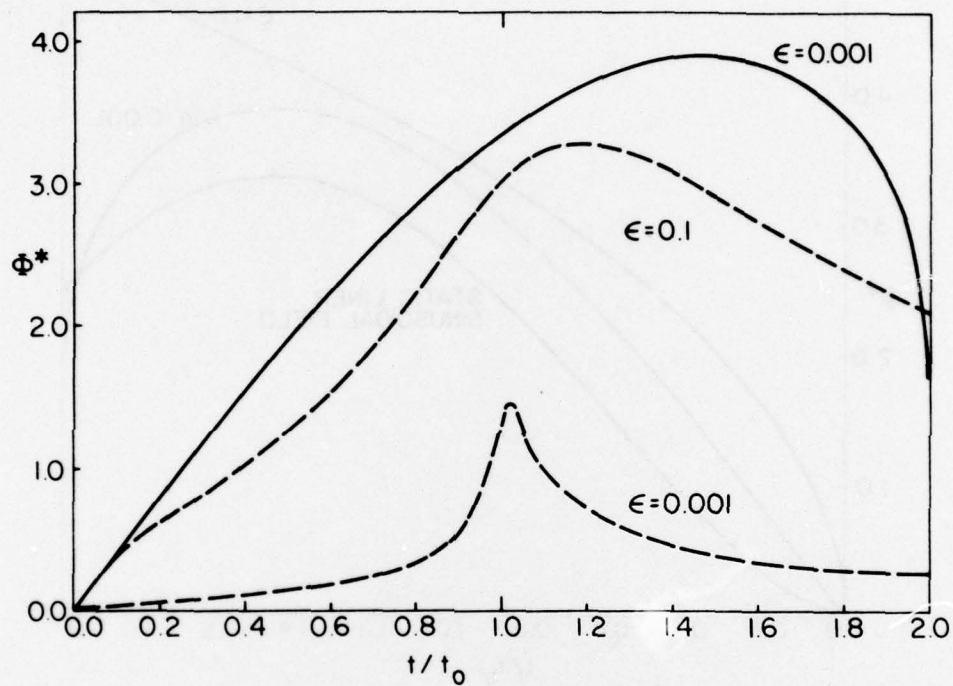


Fig. 4 — Scaled total diffused flux $\Phi^* = \Phi Rm^{1/2}/B_0 R_0^2$ as a function of t/t_0 for the two parabolic trajectories (broken trace) and one sinusoidal trajectory of Fig. 3

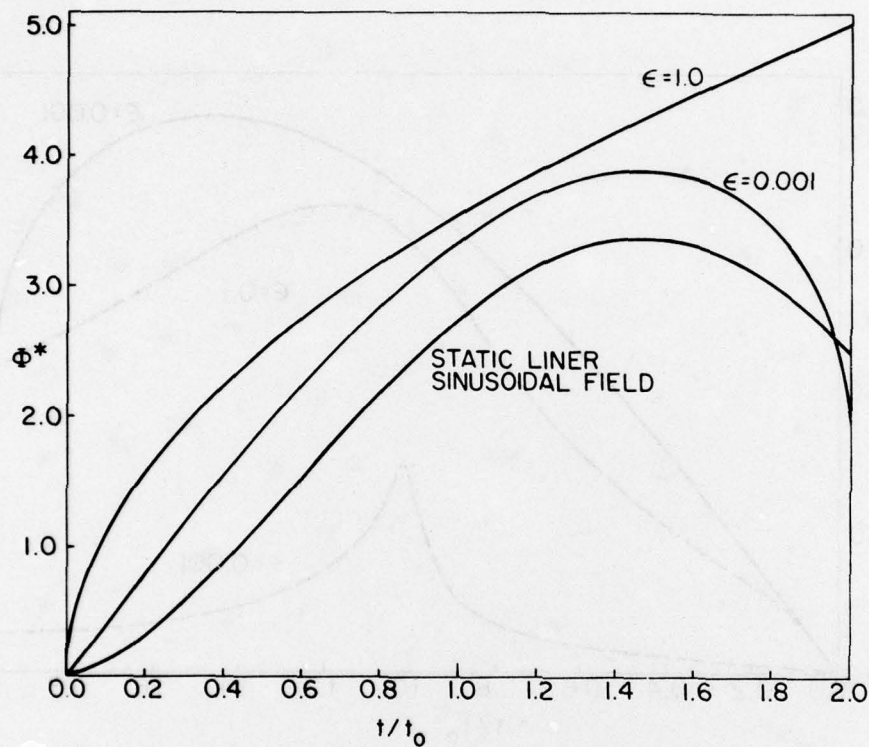


Fig. 5 — Comparison of scaled total diffused flux Φ^* as a function of t/t_0 for (a) static liner, constant vacuum field $B = B_0$ (top trace); (b) $\epsilon = 0.001$ sinusoidal trajectory and corresponding vacuum magnetic field, shown in Fig. 3 (middle trace); and (c) static lines with sinusoidal ($\epsilon = 0$, non-self-consistent) vacuum field (bottom trace).

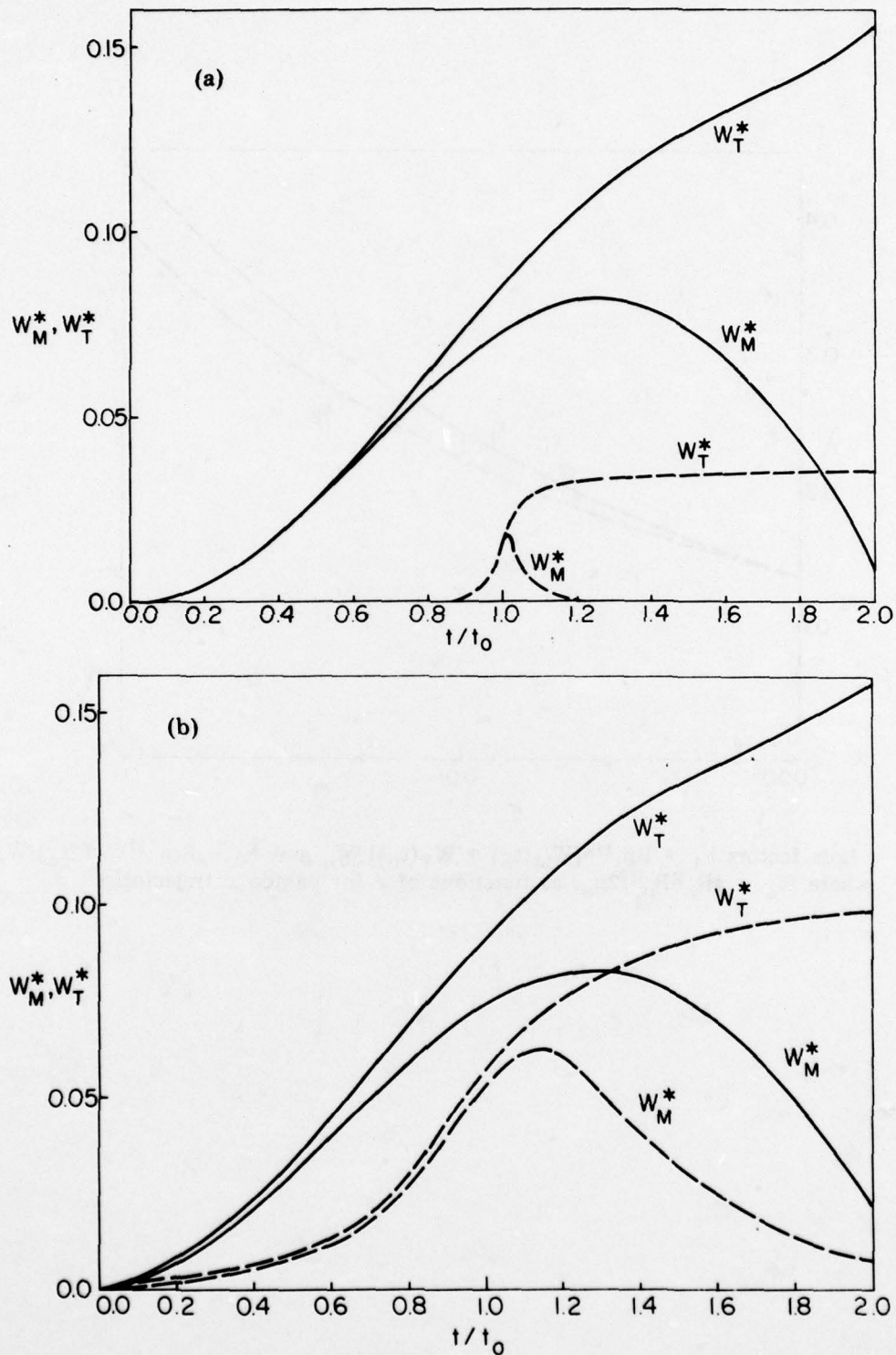


Fig. 6 — Plots of $W_M^* = W_M Rm^{1/2}/B_0^2 R_0^2$ and $W_T^* = W_T Rm^{1/2}/B_0^2 R_0^2$ scaled total magnetic and thermal energies, respectively) vs. time for (a) $\epsilon = 0.001$ and (b) $\epsilon = 0.1$. Solid lines are used for sinusoidal trajectories, broken lines for parabolic.

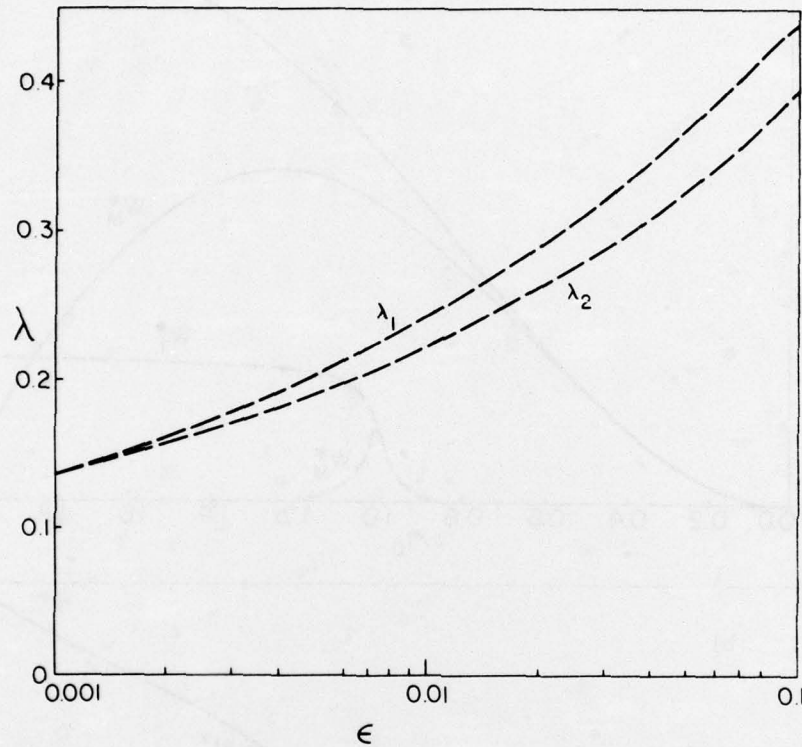


Fig. 7 — Loss factors $\lambda_1 = Rm^{1/2}[W_M(t_o) + W_T(t_o)]/W_o$ and $\lambda_2 = Rm^{1/2}W_T(2t_o)/W_o$, where $W_o = \pi R_o^2 B_o^2 / 2\mu_o$, as functions of ϵ for parabolic trajectories

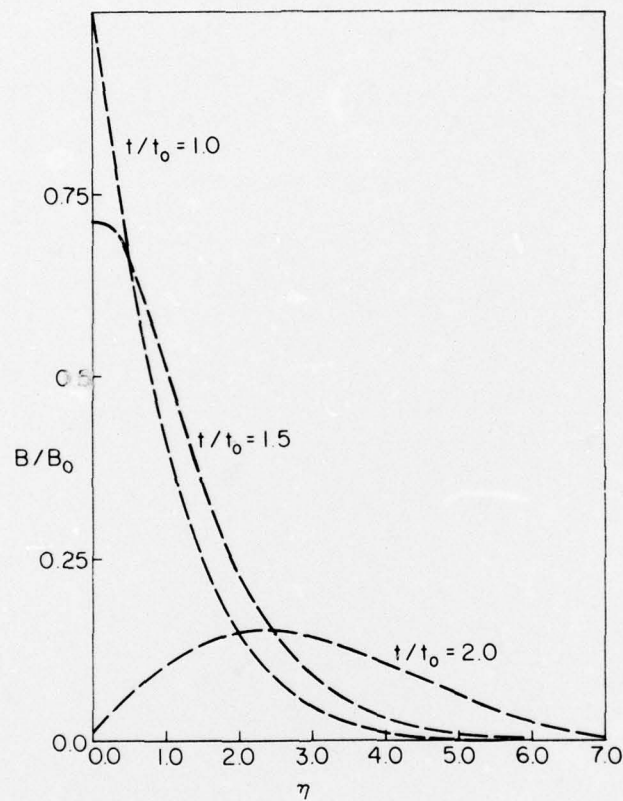


Fig. 8 — Radial profiles (B/B_0 vs η) for a parabolic trajectory at three different times $\tau = t/t_0 = 1.0$ (turnaround), 1.5, and 2.0 (return)

DISTRIBUTION LIST

- A. Administrative Agencies and Foundations
- B. Navy
- C. Government Laboratories
- D. Universities
- E. Industrial Research
- F. International

A. Administrative Agencies and Foundations

- 1. Energy Research and Development Administration
Germantown, Maryland 20767

ATTN: S. O. Dean	R. Price
G. Hess	W. Sadowski (3 copies)
R. L. Hirsch	D. Priester
B. Miller	A. Sleeper
R. Blaken	A. Davies
J. F. Decker	E. E. Kinter
J. M. Williams	

- 2. National Science Foundation
Washington, D. C. 20550

ATTN: E. C. Creutz	R. Isaacson
R. Sinclair	

- 3. Electric Power Research Institute
3412 Hillview Avenue
P. O. Box 10412
Palo Alto, California 94303

ATTN: F. F. Chen	B. D. Stetzer
------------------	---------------

B. Navy

1. Naval Research Laboratory
Washington, D. C. 20375

ATTN: Code 7700- T. Coffey (25 copies)
7701- J. Brown
7142- D. Spicer
7750- V. Grishkot (150 copies)
7708- A. E. Robson
7000- H. Rabin
6390- L. E. Steele
6390- F. Smidt

2. Office of Naval Research
800 N. Quincy Street
Arlington, Virginia 22217

ATTN: Code 420- T. G. Berlincourt
473- J. H. Satkowski

3. Pentagon
Washington, D. C. 20301

ATTN: Room 4E471- S. Koslov
4C453- P. Waterman
5D772- B. Petrie

4. Defense Advanced Research Projects Agency
Architect Building
1400 Wilson Blvd.
Arlington, Virginia 22217

ATTN: D. W. Walsh

C. Government Laboratories

1. Argonne National Laboratory 2. Brookhaven National Laboratory
9700 Cass Avenue Upton, New York 11973
Argonne, Ill. 60439

ATTN: W. Stacey

ATTN: J. Powell

3. Lawrence Livermore Laboratory
University of California
Livermore, California 94551

ATTN: K. Fowler
D. Baldwin
H. Berk
J. Killeen
B. McNamara

R. Post
J. Byers
W. Kruer
E. Valeo
B. Langdon

D. Cornish
R. Moir
C. Taylor
C. Alonso
F. Coensgen

4. Los Alamos Scientific Laboratory
P. O. Box 1663
Los Alamos, New Mexico 87344

ATTN: F. L. Ribe
C. Nielson
J. Friedberg
J. Kindell

B. Godfrey
W. Ellis
E. Lindman
H. R. Lewis

F. Tahoda
J. Marshall
K. Thomassen
J. U. Brackbill

5. Oak Ridge National Laboratory
P. O. Box X
Oak Ridge, Tennessee 37830

ATTN: J. Clarke
J. Callen
J. Hogan
R. Dory

J. Rome
G. Bateman
C. Beasley
M. Roberts

L. Berry
H. Long
D. McAlees
C. Crume

6. Princeton University
Plasma Physics Laboratory
Princeton, New Jersey 08540

ATTN: M. B. Gottlieb
R. Ellis
F. Perkins
D. Grove
H. Okuda
P. Rutherford
J. M. Greene

D. Jassby
W. Tang
H. Furth
R. Kulsrud
R. Mills
C. Oberman

J. File
E. Frieman
J. Johnson
D. Meade
T. K. Chu
T. Stix

D. Universities

1. College of William and Mary
Williamsburg, Virginia 23185

ATTN: S. P. Gary
Fred Crownfield

2. Cornell University
Ithaca, New York 14850

ATTN: Prof. R. N. Sudan (App. Phys.)
Prof. E. Ott (E. E.)
R. V. Lovelace
C. Wharton

3. Institute for Advanced Study
Olden Lane
Princeton, New Jersey 08540

ATTN: M. Rosenbluth

4. Massachusetts Institute of Technology
77 Massachusetts Avenue
Cambridge, Mass. 02139

ATTN: B. Coppi (Phys.) L. Lindsky
J. McCune (A. E.) D. Rose
A. Bers (E. E.) T. H. Dupree (Nuc. Eng.)

5. New York University
Courant Institute of Math. Sci.
251 Mercer Street
New York, New York 10012

ATTN: H. Grad
W. Grossman
H. Weitzner
J. Tataronis

6. Stevens Institute of Technology
Hoboken, New Jersey 07030

ATTN: George Schmidt
B. Rosen

7. University of California
Berkeley, California 94720

ATTN: Prof. A. Kaufman
Prof. C. K. Birdsall

8. U.C.L.A.
Los Angeles, California 90024
ATTN: J. Dawson (Phys.) B. Fried (Phys.)
Y. C. Lee F. Chan (E. E.)
9. University of Maryland
College Park, Maryland 20742
ATTN: P. C. Liewer C. S. Liu
Prof. R. Davidson H. Griem
10. University of Rochester
Rochester, New York 14627
ATTN: Moshe Lubin A. Simon
L. Goldman R. McCrory
P. J. Gatto
11. University of Texas
Austin, Texas 78712
ATTN: D. Ross F. Hinton
W. Drummond W. Horton
A. Ware R. Hazeltine
L. Sloan
12. University of Wisconsin
Madison, Wisconsin 53706
ATTN: R. Conn G. Kulcinski
R. Boom
13. Yale University
New Haven, Conn. 06520
ATTN: B. Bernstein

E. Industrial Research

1. Batelle
Pacific Northwest Lab.
P. O. Box 999
Richland, Washington 99352

ATTN: L. Schmidt
2. Bell Telephone Laboratories
Whippany, New Jersey 07981

ATTN: S. Buchsbaum A. Hasegawa
3. Forsen Incorporated
777-106 Avenue, N. W.
Bellevue, Washington 98004

ATTN: H. Forsen
4. General Atomic Company
P. O. Box 81608
San Diego, California 92138

ATTN: T. Ohkawa C. Baker
D. Dobrott J. Purcell
G. Guest
5. Maxwell Laboratories, Incorporated
9244 Balboa Avenue
San Diego, California 92123

ATTN: A. Kolb A. Trivelpiece
V. Fargo N. Rostoker
6. Physics International Company
San Leandro, California 94557

ATTN: V. Bailey
7. Sandia Laboratory
Albuquerque, New Mexico 87115

ATTN: Thomas Wright J. Freeman

8. Science Applications, Inc.
Laboratory for Applied Plasma Physics
Research Staff
La Jolla, California 92037

ATTN: N. Krall C. Wagner
 R. Shamy H. Klein
 J. McBride N. Byrne

9. Westinghouse Electric Company
Breeder Reactor Division
P. O. Box 355
Pittsburgh, Pennsylvania 15230

ATTN: Z. Shapiro D. Klein
 R. Rose T. Varljen

10. Fusion Energy Corporation
P. O. Box 2005
Princeton, N. J. 08540

ATTN: B. C. Maglich R. A. Miller

F. International

1. Australian National University
Canberra A. C. T. Australia

ATTN: J. D. Strachan R. L. Dewar

2. Center d'Etudes Nucleaires
Boite Postale No. 6
92260 Fontenay-Aux-Rose
France

ATTN: J. Tachon N. Trocheris
C. Mercier R. B. Paris

3. Centro di Studio sui Gas Ionizzati
Universita di Padova
6/a Via Gradenigo
35100 Padova, Italia

ATTN: G. Malesani G. Nalesso

4. Culham Laboratory
Abingdon, Berkshire, England

ATTN: Chris Lashmore Davies R. Bickerton
I. Cook M. Hughes
K. Roberts J. A. Wesson
J. Christiansen T. Stringer
J. B. Taylor J. W. M. Paul
B. Peas A. Gibson
R. Rebut

5. Institute of Plasma Physics
Nagoya University
Furo-cho, Chikusa-ku
Nagoya 464, Japan

ATTN: S. Hiroe T. Dawamura
H. Ikegami T. Kawabe

6. Japan Atomic Energy Research Institute
Tokai-mura, Naka-gun
Ibaraki 319-11
Japan

ATTN: N. Fujisawa

7. Kurchatov Institute
Moscow, U. S. S. R.
ATTN: B. B. Kadomtsev E. P. Velikov
L. I. Rudakov
8. Laboratoria di Fisica
Via Celoria 16
20133 Milano, Italia
ATTN: P. Caldirola E. Sindoni
9. Max Planck Institute fur Plasma Physics
8046 Garching bei Munchen
West Germany
ATTN: D. Biskamp K. Von Hagenow
Horst Pacher Chodura
W. Schneider D. Pfirsch
10. Siberian Nuclear Physics Institute
Novosibirsk, U. S. S. R.
ATTN: D. D. Ryutov
11. University of Natal
King George V Avenue
Durban, South Africa
ATTN: M. A. Hellberg
12. CNEN, Laboratory Gas Ionizzati
C. f. 65, 00044 Frascati:
Rome, Italy
ATTN: R. Toschi
13. FOM-Instituut voor Plasmafysik
Rijnhuizen, P. O. Box 7
Jutphaas, Netherlands
ATTN: C. M. Braams F. Engelman